Valorization of dredged sediments in self-consolidating concrete: Fresh, hardened, and microstructural properties

A.E.M. Safhi, P. Rivard, A. Yahia, M. Benzerzour, K.H. Khayat

Valorization of Dredged Sediments in Self-Consolidating Concrete: Fresh, Hardened, and Microstructural Properties

Amine el Mahdi Safhi [(1) (2) (*)], Patrice Rivard [(1)], Ammar Yahia [(1)], Mahfoud Benzerzour [(2)]; Kamal Henri Khayat [(3)]

[(1)] Université de Sherbrooke, Department of Civil and Building Engineering, Sherbrooke, Canada

[(2)] IMT-Lille-Douai, Laboratoire de Génie Civil et géo-Environnement (LGCgE), Douai, France

[(3)] Missouri S&T, Center for Infrastructure Engineering Studies, Rolla, MO, USA

[(*)] Corresponding author: Amine el Mahdi Safhi

Email: amine.el.mahdi.safhi@usherbrooke.ca

Address: Université de Sherbrooke – Faculty of Engineering - Department of Civil and Building Engineering, 2500, boulevard de l'Université, Sherbrooke (Québec) J1K 2R1, Canada

Word count: 7413

Valorization of Dredged Sediments in Self-Consolidating Concrete: Fresh, Hardened, and Microstructural Properties

Abstract

Several studies have proven the use of dredged sediments as supplementary cementitious materials (SCMs), but limited information is available on the effect of such treated sediments on self-consolidating concrete performance. The main objective of this study was to evaluate the performance of self-consolidating concrete (SCC) fabricated with treated sediments. The sediments were thermally treated at 800 °C for 1 h. The packing density of the granular skeleton was optimized to reduce the paste content and produce SCC with relatively low binder content. Three different SCC mixtures were prepared with 0%, 10%, and 20% cement replaced with treated sediments by mass. Key fresh, physical, hardened, and microstructural properties of the investigated SCC mixtures subject to different curing regimes were evaluated. The test results showed that the optimized SCC mixtures exhibited adequate self-consolidation characteristics. The particle size and high chemical activity of the sediments led to pore refinement of micro-pores, increased density, improved microstructure, and reduced micro-cracks of the investigated SCC mixtures. Furthermore, the use of up to 20% of treated sediments resulted in a compressive strength of 66 ± 1 MPa at 91 days, which is comparable to that of the reference mixture made without any sediments. Leaching test results confirmed the ecological potential of producing SCCs based on sediments, which could be an interesting alternative of using local materials to reduce the high demand of cement, thus further reducing the CO_2 footprint of concrete structures.

Keywords: Dredged sediments; Mechanical properties; Packing density; Self-consolidating concrete; Supplementary cementitious material; Ultrasonic pulse velocity.

1. Introduction

Self-consolidating concrete (SCC) can be used to facilitate concrete mixing and placement and ensure proper filling of complex frameworks without any mechanical consolidation. This can help reduce cost, labor, and construction time and provide more freedom in the design and enhancement of surface finish (Khayat et al., 1999). The design of stable SCCs can enhance the interfacial transitional zone (ITZ) properties with embedded reinforcement and with aggregates that can lead to greater SCC performance (Khayat et al., 1999). One of the drawbacks of SCC is its higher content of fine powder attributed to the relatively high-binder content than that in conventional concrete. Extensive research has been conducted on the feasibility of valorizing abundantly available by-products as supplementary cementitious materials (SCMs) to partially replace cement and reduce the environmental footprint of SCC. Commonly used SCMs are fly ash, ground-granulated blast-furnace slag, silica fume, limestone filler, marble powder, calcined clay, palm oil fuel ash (Mohammadhosseini et al., 2015), and waste ceramic nanoparticles (Lim et al., 2018). These materials are primarily composed of silicon dioxide (SiO_2), aluminum oxide (Al_2O_3), and calcium oxide (CaO). The presence of additional oxides can be beneficial to produce additional pozzolanic calcium-silicate-hydrate (C-S-H) gel.

Significant volumes (more than one billion cubic meter) of dredged sediments are produced worldwide every year (Benzerzour et al., 2017). These materials are stored or disposed at sea when they are not contaminated. However, these sediments are very heterogenous: the provenance and dredging time during the year have a crucial influence on their composition. This makes each sediment a unique material which requires special treatment. The valorizing of dredged sediments in concrete, engineered materials, and civil engineering applications presents considerable benefits. Such valorization includes the fabrication of bricks (Samara et al., 2009), ceramic products (Xu et al., 2014), lightweight aggregates (Liu et al., 2018), and road construction materials (Kasmi et al., 2017). Recent studies have demonstrated that thermally treated sediments can render the sediments

more reactive and that treated sediments can be useful for clinker production (Aouad et al., 2012; Faure et al., 2017) or as SCM.

Dang et al. (2013) designed a new blended cement containing 8%, 16%, and 33% of treated sediments from the trap Lyvet on the Rance River in France. The sediments were heated at 650 °C and at 850 °C for 5 h. Blended cements containing 8% treated sediments secured equivalent long-term compressive strength compared with the reference mixture made without any sediment. The authors reported that the composite binder required a longer curing period for the development of mechanical properties. Ez-zaki and Diouri (2019) investigated the microstructural and physic-mechanical properties of mortars made with 8% and 33% thermally treated sediments and shell powder at 650 and 850 °C for 5 h. Despite the pozzolanic reactivity of treated sediments, the compressive strength of the mixtures containing the treated sediment was lower than that of the control mortar. Van Bunderen et al. (2019, 2017) studied the early-age hydration and autogenous deformation of cement paste containing 20%, 30%, and 40% of flash calcined dredging sediments treated at 865 °C. The treated sediments and fly ash developed a similar early-age hydration behavior, and the addition of sediments reduced the autogenous shrinkage of mortar. Snellings et al. (2017, 2016) studied the pozzolanic reactivity of flash calcined sediments (from the port of Antwerp, Belgium) treated at temperatures of 820, 865, and 905 °C. The pozzolanic reactivity of sediments was found to be inferior to that of metakaolin but was superior of that of siliceous fly ash in a calorimetry based pozzolanic reactivity test. Zhao et al. (2018) investigated the effect of using 10%, 20%, and 30% cement replacement of uncontaminated sediments on properties of mortar and concrete mixtures. The reported results showed that dried and finely ground sediments can be used as partial substitutes of cement by up to 20% without hindering the mechanical properties of the mixtures. Benzerzour et al. (2018, 2017) developed a new blended cement containing 8% and 15% sediments thermally treated at temperatures of 650, 750, and 850 °C for different durations ranging between 1 and 3 h. Test results showed that mortar mixtures incorporating 15% sediments treated at 850 °C for 1 h developed better mechanical strength than the control mortar.

Although various non-traditional by-products have been recycled to SCC, such as waste carpet fibers and palm oil fuel ash (Mohammadhosseini et al., 2018, 2017), limited research has been conducted on the engineering properties of SCC incorporating the treated sediments. Sediments used as fillers in SCC achieved good performance (Rozas et al., 2015; Rozière et al., 2015). Bouhamou et al. (2016) evaluated the influence of using 10%, 15%, and 20% replacements of cement by calcined dam mud sediments treated at 750 °C for 5 h on the shrinkage of SCC. They reported that the increase in calcined mud content resulted in more viscous and less workable SCC for a given water content. A higher mechanical strength of SCC containing 10% calcined mud was reported. However, notably, the control SCC mixture exhibited the highest strength development. It was also reported that the addition of calcined mud resulted in lower autogenous shrinkage. This was attributed to the formation of expansive calcium aluminate hydrates, which compensated for the shrinkage. Nevertheless, the effect of sediments on fresh, hardened, and microstructural properties of SCC are still not well understood.

2. Research significance

The present study is part of a wide investigation aimed at evaluating the feasibility of using dredged marine sediments from Dunkirk Port as SCM in SCC mixtures. Valorizing the sediments using high-fluid cement paste mixtures at different substitution rates did not significantly affect the fresh properties of paste when the water demand of sediments was considered (Safhi et al., 2018). The study showed that the treated sediments can be used for partial replacement of cement by up 30%. Another study conducted on equivalent-SCC mortar mixtures confirmed the previously reported results (Safhi et al., 2019). However, although the treated sediments are considered as pozzolanic materials, the use of higher substitution rate reduced the strength and modulus of elasticity of SCC mortars. Optimum replacement rates of 7% and 35% in the case of binder content ranging between 380 and 600 kg/m^3 and w/cm of 0.32 and 0.34, respectively, were reported.

The main objective of this study is to obtain deeper insights into the effect of using treated sediment on the fresh, physical, hardened, and microstructural properties of SCC proportioned with

a fixed binder content of 450 kg/m^3. A leaching test was conducted to evaluate the potential of producing SCC containing recycled sediments.

3. Materials and experimental program

3.1. Material characteristics

The investigated SCC mixtures were fabricated using a ternary binder containing approximately 70% General Use (GU) cement, 25% class F fly ash, and 5% silica fume. Two crushed coarse aggregates (CA), including CA_1 and CA_2 with nominal maximum sizes of 20 and 10 mm, respectively, were used. The CA_1 and CA_2 aggregates, from St Dominique career, had a specific density of 2.76 and 2.72, water absorption values of 0.48% and 0.41%, and bulk densities of 1465 and 1444 kg/m^3, respectively. A siliceous river sand with a specific density of 2.66, a water absorption of 1.09%, and a bulk density of 1785 kg/m^3 was used.

The sediments used in this study were extracted from the Port of Dunkirk in France. They were dried in an oven at 60 °C and subsequently sieved to recuperate fine particles smaller than 2 mm. Thermogravimetric analysis (TGA) was performed using NETZSCH STA 449 and nitrogen gas in a controlled environment with argon flow (75 ml/min) at variable temperatures ranging between 105 and 1100 °C at an increasing rate of 2 °C/min. Differential thermal analysis was also performed using NETZSCH DSC 404F3 at ambient air and variable temperatures (0 to 1000 °C, at a range of 5 K/min/1000). As can be observed in Fig. 1, the first weight loss around 300 °C was due to the evaporation of water and dehydration of gypsum (Siavalas et al., 2013). The weight loss of 3.2% observed between 400 and 500 °C was due to the combustion of carbon and organic matter, as shown by the increase in the released carbon. This loss was associated with an exothermal peak. A higher weight loss between 550 and 750 °C was observed, which was associated with an endothermic peak due to the decomposition of calcite ($CaCO_3$) (Madrid et al., 2017). Above 800 °C, the weight loss and calorimetry flux tended to stabilize, which confirmed that almost all organic matter was eliminated. Calcination at 800 °C for 1 h was chosen as the thermal treatment.

After calcination, the powder was ground and then sieved to meet a d_{50} of less than 45 µm, and the obtained product was referred to as treated marine sediment (TMS). The visual aspect of those sediments at the various stages of treatment is shown in Fig. 2. The physical and chemical characteristics of the ternary binder, raw sediments, and TMS are summarized in Table 1. Calcination had a beneficial effect in that it increased the density of the sediments through the elimination of organic matter. The sediments were also chemically activated with an increase in silica (+37%), despite the decrease in the concentration of aluminum, calcium, ferric, and magnesium oxides. Silicon dioxide can react with calcium hydroxide (CH) to form additional pozzolanic (C-S-H) gel. The content of Fe_2O_3 and K_2O indicates the presence of illite. The changes in the colors of sediments after calcination were due to the decrease of Fe_2O_3 content from 9.7% to 5.3%. Notably, a decrease in sulfur trioxide (SO_3) content was observed, which decreased the risk of delayed ettringite formation. The particle-size distributions of the CA, sand, cement, and TMS are shown in Fig. 3. As can be observed, the particles of TMS have a spherical morphology.

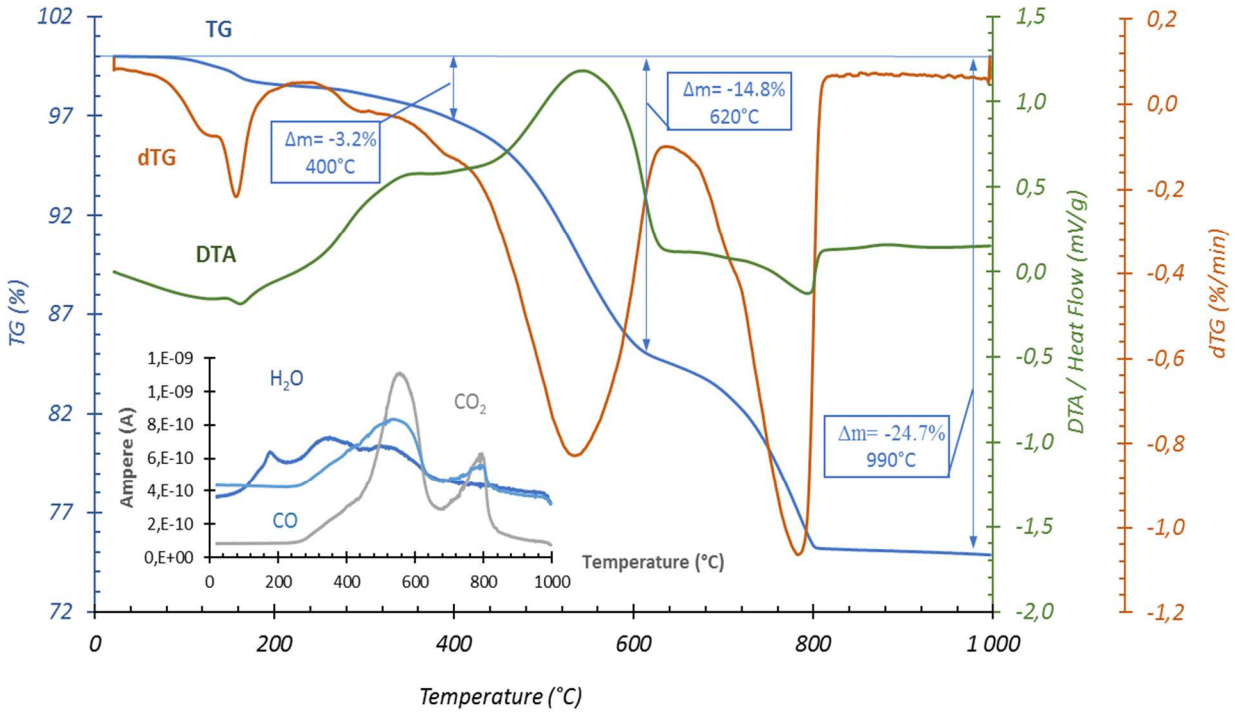

Fig. 1 : TGA-DSC curves of raw sediments

141

142 *Fig. 2 : Visual aspect from the left to right: raw dried sediment; calcined, ground sediments*

143 *Table 1 : Physio-chemical characteristics of powders*

Characteristics		***Ternary binder***	***Raw Sediments***	***TMS***
Physical properties	*Density (kg/m³)*	2888	2467	2704
	BET Surface Area (m²/kg)	2535	-	3143
Major oxide (wt %)	Al_2O_3	8.54	4.12	3.85
	CaO	43.1	11.4	9.73
	Fe_2O_3	6.46	9.75	5.32
	MgO	1.62	0.96	0.76
	P_2O_5	0.14	0.14	0.14
	SO_3	3.39	1.49	0.30
	SiO_2	29.4	52.3	71.9
	TiO_2	0.41	0.42	0.27
	K_2O	1.09	0.95	1.07
	Na_2O	0.26	0.66	0.73
	Alkali equivalent $Na_2O + 0.658 \times K_2O$	0.98	1.29	1.43
	Other undetected oxides	1.68	0.64	0.67
	LOI (1050°C)	3.75	16.9	5.18

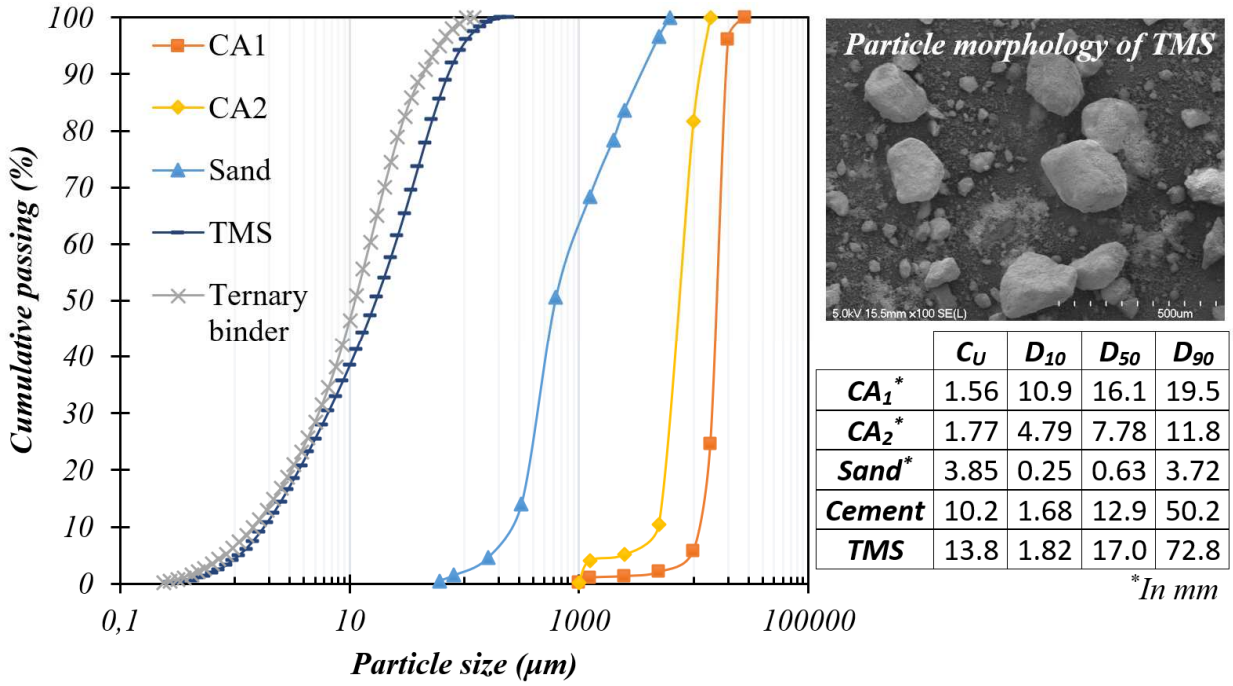

	C_U	D_{10}	D_{50}	D_{90}
CA_1*	1.56	10.9	16.1	19.5
CA_2*	1.77	4.79	7.78	11.8
Sand*	3.85	0.25	0.63	3.72
Cement	10.2	1.68	12.9	50.2
TMS	13.8	1.82	17.0	72.8

*In mm

Fig. 3 : Particle-size distributions of powders and aggregates

3.2. Packing density of aggregate

The packing density (PD) of the aggregate was determined to minimize the paste content and produce SCC with a relatively low binder content. Enhancing the PD can also reduce the high-range water reducing admixture (HRWRA) demand and the viscosity of the concrete (Khayat et al., 2002) and can increase the static stability, compressive strength (Aïssoun et al., 2016), and modulus of elasticity. A high PD can reduce porosity, chloride diffusion, and shrinkage (Abd Elrahman and Hillemeier, 2014). The PD was experimentally determined using a modified version of the test procedure described in ASTM C29 (2017). It involved determining the PD of materials poured from a V_{funnel} into a recipient. The used V_{funnel} had an upper opening of 75 × 515 mm^2 and an outlet opening of 75 × 65 mm^2, as described by the EFNARC (Self-Compacting Concrete European Project Group, 2005). A 7-l cylindrical container with a diameter of 200 mm was used as the recipient. Goltermann et al. (1997) suggested that the diameter of the cylinder should be larger than 10 times the nominal maximum size of the aggregate. Nanthagopalan and Santhanam (2012) used the same test procedure with different test setups.

To establish a compact granular skeleton, a mixture design approach based on varying the fine and coarse aggregate, CA_1, CA_2, and sand at volumetric proportions from 0 to 100% was used. Different volumetric proportions of CA_1, CA_2, and sand were manually mixed and used to determine the PD according to the ENFRAC method. The premixed aggregate combinations were placed in the V_{funnel} and poured into the container from a height of 0.20 m without any vibration. The exceeded quantity was stricken off, and the mass of the filled container was measured. As can be observed in Fig. 4, the experimental data, in which each red point represented 16 different combinations of aggregates, were used to establish the corresponding contour diagrams (red points in Fig. 4). Using the proportions, the reel masses of each component and the voids content were determined, and then, the PD values were calculated as follows:

$$Packing\ Density = 1 - Void\ content = 1 - \frac{(V_{container} - V_{CA1} - V_{CA2} - V_S)}{V_{container}} \qquad Eq.\ 1$$

where $V_{container}$, V_{CA1}, V_{CA2}, and V_S are the volumes of the used container, CA_1, CA_2, and sand. The quadratic multi-regression model showed the best fit for the experimental measurement ($R^2 = 0.980$, a p-value < 0.001, and a low standard deviation of 0.01). Depending on the selected aggregate combination, the PD varied from 0.530 to 0.720. The sand was found to be the most dominant parameter. The optimal PD of 0.72 was reached by different combinations of aggregates as shown in Fig. 4. Following the recommendations of EFNARC to produce SCCs ($48 \leq V_{FA}/V_A \leq 55\%$), a higher PD of 0.72 could not be directly assumed; then, a PD of 0.70 was chosen. This PD can be achieved using 893 kg/m^3 of sand, 147 kg/m^3 of CA_1, and 578 kg/m^3 of CA_2, which correspond to 55%, 10%, and 40% by volume, respectively.

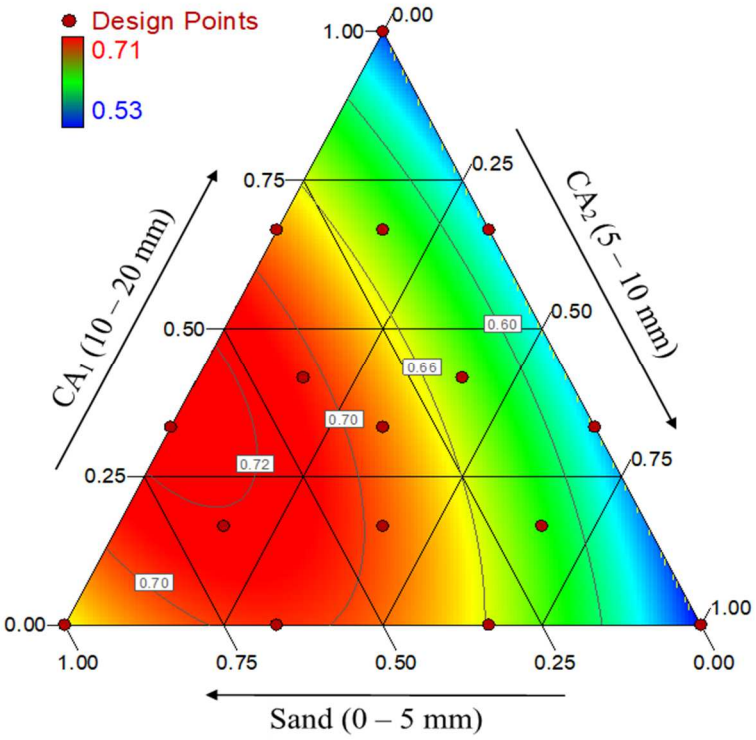

Fig. 4: Ternary PD diagram, the red points represent experimental measurements

3.3. Mixtures proportioning

Three SCC mixtures were prepared with 0 (SCC-R), 10% (SCC-1), and 20% (SCC-2) cement replaced with TMS by mass (Table 2). The mixtures were prepared with a constant water-to-cementitious materials ratio (w/cm) of 0.40. The water demand of sediments was calculated according to the method reported by Sedran et al. (2007). A commercially compatible HRWRA was used at an optimum dosage of 1200 ml/100 kg of binder to secure the targeted slump flow (S_{flow}) of 680 ± 20 mm.

All the investigated mixtures were prepared in a rotating drum mixer in batches of 60 l. The mixing sequence was as follows: homogenizing sand for 30 s, followed by adding coarse aggregate and mixing for 60 s. One third of the water was then added, and the material was mixed for 30 s. The cementitious materials were added and mixed for 30 s before introducing HRWRA diluted with one third of the water. The concrete was then mixed for an additional 120 s followed by the addition of the last portion of water. The concrete was mixed for 60 s and left to rest for 2 min, after which the mixing was resumed for another 3 min.

196 *Table 2 : Mixture proportions of the investigated SCC mixtures*

Materials	***SCC-R***	***SCC-1***	***SCC-2***
	Content in kg/m^3		
Cement	450	405	360
TMS	-	45.0	90.0
CA_1	147		
CA_2	578		
Sand	893		
Water (w/cm = 0.4)	180	162	144
Added water (w/s =0.35)	-	15.7	31.5

197 # 4. Results and discussion

198 ## 4.1. Fresh properties

199 Before casting, fresh property tests (e.g., S_{flow} diameter, T_{500}, V_{funnel} time, J_{Ring} diameter, L-
200 box, resistance to static segregation, and air content) were performed according to the EFNARC
201 guidelines. The fresh properties of the investigated SCC mixtures are summarized in Table 3. The
202 SCC mixtures achieved a S_{flow} ranging between 685 and 695 mm, which corresponded to SCC class
203 2 (SF2) based on EFNARC. A slight decrease in S_{flow} was observed when the TMS content
204 increased, which could be explained by the increase in their specific surface area. Laidani et al.
205 (2020) found that fine calcined bentonite particles decreased the S_{flow} because of the increased
206 particle surface area of bentonite compared to OPC. All the SCCs exhibited a similar T_{500} value of 2
207 s, and the V_{funnel} flow time ranged between 6 and 8 s, which agrees with the fresh density (which
208 increased with increasing TMS content). The H_2/H_1 ratio was determined to evaluate the self-
209 leveling properties, blocking, and stability of concrete (Khayat et al., 2004). The results of L-box
210 flow show that the H_2/H_1 ratio ranged between 0.85 and 0.98, and the Δ between S_{flow} and J_{Ring} flow
211 was < 50 mm. The findings indicate that all mixtures have a good passing ability and were within

212 the targeted range. The segregation index ≤ 10% and the Δ between initial and final V_{funnel} flow ≤
213 10% indicates the good stability of the studied SCCs.

214 *Table 3: Results of fresh properties of SCCs*

Properties		***SCC-R***	***SCC-1***	***SCC-2***
Filling ability	*S_{flow} (mm)*	695	690	685
	T_{500} (s)	2.00	2.03	2.06
	Initial V_{funnel} time (s)	8.10	7.41	6.66
Passing ability	*J_{Ring} flow (mm)*	655	662	665
	L-box flow	0.98	0.94	0.85
Stability	*Δ_t initial & final V_{funnel} (%)*	5.43	3.37	9.31
	Sieve segregation (%)	6.59	8.47	6.23
Air content (%)		3.90	2.20	1.38
Fresh density (kg/m^3)		2310	2366	2376

215 **4.2. Physical properties**

216 **4.2.1. Thermal calorimetry kinetics**

217 Paste mixtures containing 0, 10, and 20% of TMS and a fixed water-to-binder ratio of 0.50
218 were prepared and used to evaluate the calorimetric flux using an isothermal calorimeter (TAM Air)
219 within 50 h according to ASTM C1679 (2017). The hydration heat evolution curves of cement-
220 sediment binders are shown in Fig. 5. Right after mixing the binder with water and because of the
221 rapid dissolution of sulfate and aluminate, a sharp exothermic peak was observed which was caused
222 by the formation of Aft (alumina, ferric oxide, tri-sulfate) linked to a rapid decrease in heat
223 emission. Addition of TMS retarded the hydration of the binder. As can be observed, the SCC-R
224 paste generated 3.27 mW/g of heat after 8.53 h, whereas SCC-1 and SCC-2 pastes released 2.96 and
225 2.77 mW/g heat after 8.63 and 8.58 h, respectively. The first endothermic peak was mainly related
226 to C_3S and C_3A hydration which formed C-S-H and ettringite, respectively. The second peak was

associated with a certain surplus or delay in C_3A hydration due to the increase in gypsum content; therefore, the ettringite transformed to monosulfate according to the following equation:

$$C_3A.3\,C-S-H_{32}+\ 2\,C_3A+4H\rightarrow 3\,C_3A.C-S-H_{12} \qquad Eq.\ 2$$

Unlike the results reported by Benzerzour et al. (2017), the incorporation of TMS reduced the heat of hydration. This contradiction can be explained by the fineness of TMS used in this study, which was coarser (d_{50} of TMS particles is 17 µm) than that (d_{50} of TMS particles is 5 µm) used by Benzerzour et al. (2017). This resulted in higher hydration kinetics of sediments. In contrast, the retarding effect was caused by the reduction of the Ca^{2+} ions, which affected the hydration kinetics, delayed $Ca(OH)_2$ nucleation, and generated an unstable C-S-H gel with low Ca/Si ratio, which slowly changed into a stable C-S-H gel (Han et al., 2014). A second possible cause could be the agglomeration of sediments, which entrapped some mixing water between flocs and reduced the available water for hydration (Oey et al., 2013).

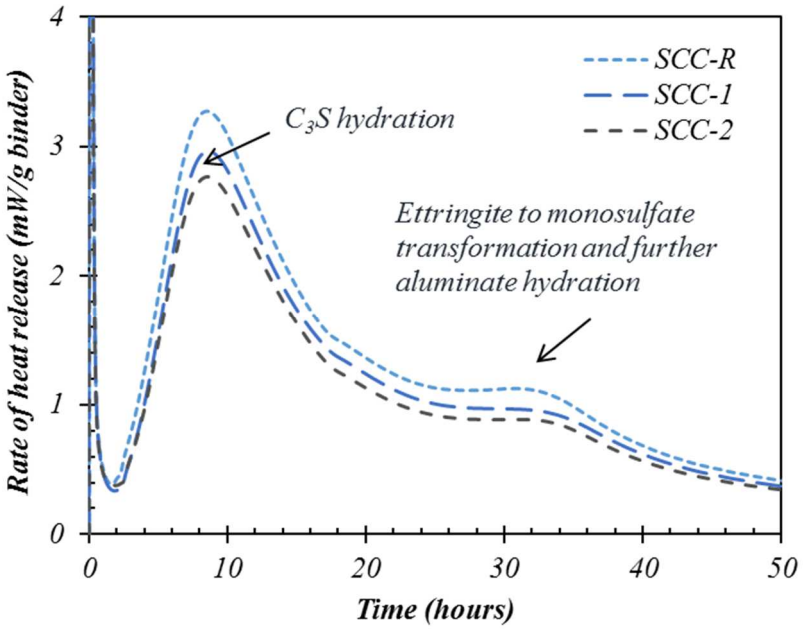

Fig. 5: Evolution of heat hydration for the different SCC mixtures

4.2.2. X-ray diffraction analysis

X-ray diffraction analyses were conducted at an age of 40 days on dried and ground pastes. Analyses were conducted using a Panalytical X'Pert Pro MPD Diffractometer equipped with CuKα

radiation (λ = 1.54 Å). Fig. 6 shows that quartz (Q), ettringite ($Ca_6Al_2S_3O_{50}H_{64}$), and portlandite ($Ca(OH)_2$) were the main phases. Some minor phases, such as gypsum ($CaSO_42H_2O$), alite (Ca_3SiO_5), calcite ($CaCO_3$), and tricalcium aluminate ($Ca_3Al_2O_6$), were also detected. The XRD analysis results agreed with the results of the thermal calorimetry kinetics with respect to the formation of ettringite. The early-age phase (9-2θ°) was a solid solution of carbonated ettringite (hemicarbonate) and OH^- substituted mono-sulfate ettringite (Van Bunderen et al., 2019).

The three samples made with different TMSs exhibited the same pattern; overall, there were no significant differences in hydration products. The greater the TMS substitution rate, the higher the intensity of diffraction peaks of quartz (21, 27, 37, 50, 60, and 68 2θ°). This result was consistent with the results of XRF analysis: the high SiO_2/Al_2O_3 ratio indicates the presence of free silica. Compared with the reference paste, the other pastes containing 10 and 20% TMS exhibited lower intensity diffraction peaks of portlandite, which can be attributed to the pozzolanic activity of sediments.

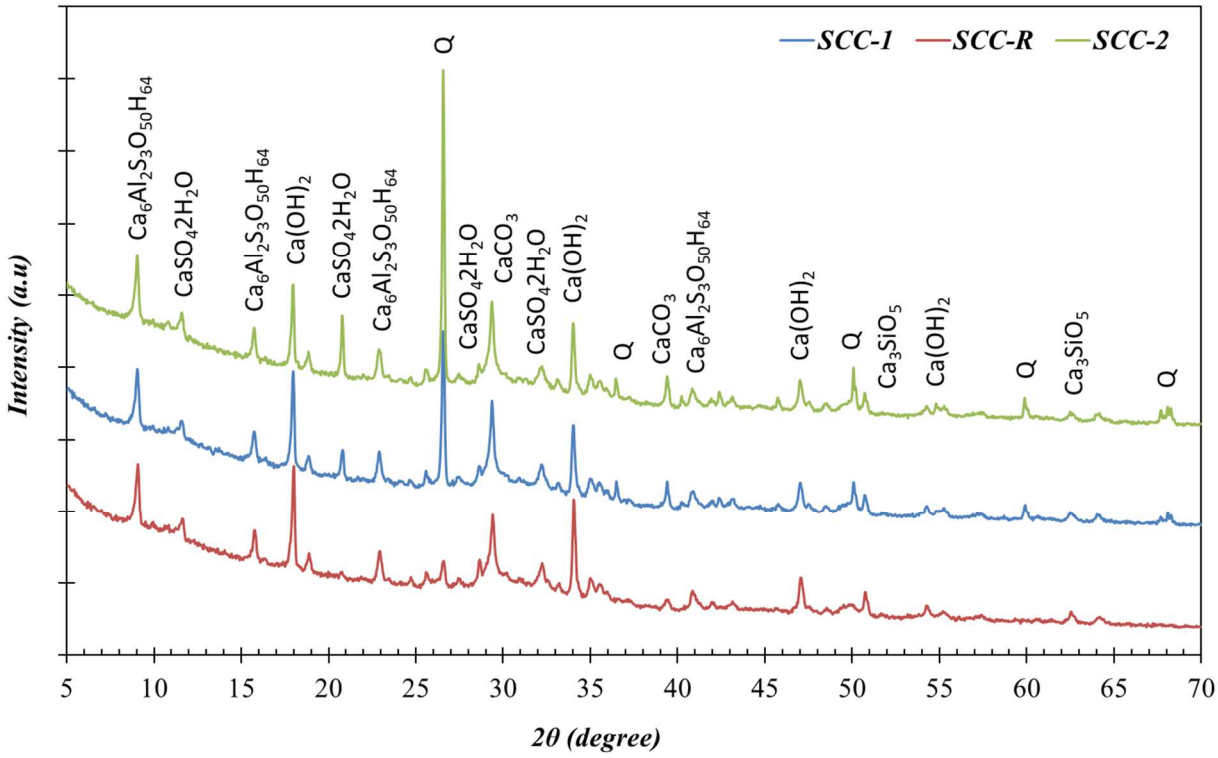

Fig. 6: XRD profiles of the different SCC pastes

259 ### 4.3. Hardened properties

260 #### 4.3.1. Compressive and splitting tensile strengths

261 Compressive strength (ASTM C39, 2018) and splitting tensile strength (ASTM C496, 2017)
262 were determined from 100 Ø 200 mm cylindrical specimens (3 samples for each test), at 3, 28, 56,
263 and 90 days. The results are presented in Fig. 7 and Fig. 8. The investigated SCC mixtures showed
264 a similar tendency of increase in strength with curing time.

265 The compressive strengths of the SCC-1 mixture made with a replacement rate of 10%
266 increased by approximately 10%, 2%, 3%, and 4% after 3, 28, 56, and 91 days, respectively.
267 However, for a replacement rate of 20%, the early-age compressive strength of the SCC-2 mixture
268 was lower than that of the control mixture but was comparable at later ages. These results are
269 consistent with data obtained in the case of SCMs, which required more curing time to develop their
270 strength. For the splitting tensile strength, the SCC-1 mixture showed a similar behavior to that of
271 SCC-R. However, at 20% replacement, the SCC-2 mixture showed a slightly lower strength at an
272 early age, which was still acceptable considering the standard deviation. According to Çakır (2014),
273 the development of the tensile splitting strength was mainly attributed to the binder rather than the
274 other ingredients. Therefore, the increase in the TMS content resulted in lower amount of hydration
275 products, which can lead to higher porosity, lower bonding strength, and weaker ITZ (Wong et al.,
276 2009).

277 The optimization of the PD and the type of aggregate had an important role on strength
278 development. Nevertheless, replacing more than the above-mentioned contents of TMS would not
279 result in a pozzolanic reaction but would deteriorate the mechanical properties.

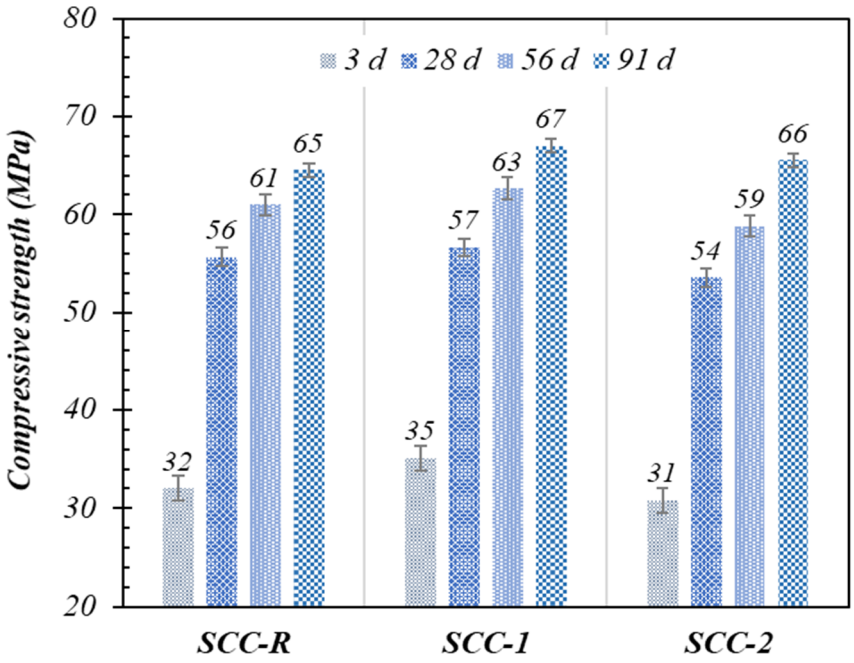

280

281 *Fig. 7: Compressive strength results of investigated SCC mixtures*

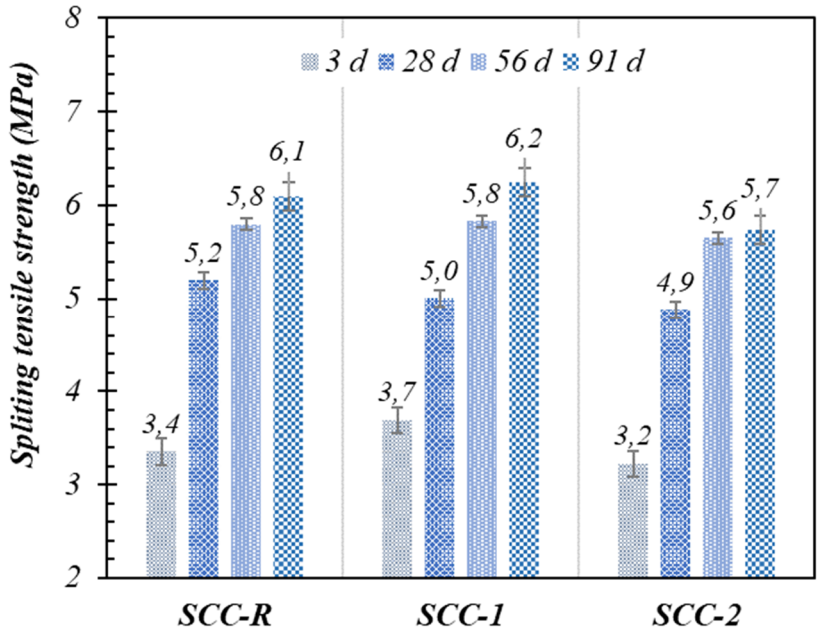

282

283 *Fig. 8: Splitting tensile strength results of investigated SCC mixtures*

284 **4.3.2. Ultrasonic pulse velocity (UPV) and dynamic modulus of elasticity**

285 The UPV is a non-destructive test that assesses the internal microstructural soundness,
286 micro-cracking, homogeneity, and compactness (Skaropoulou et al., 2013). UPV is associated with
287 micro-crack formation in concrete (Ashrafian et al., 2018). UPV was performed according to

ASTM C597 (2016) on the specimens tested for compressive strength. The dynamic modulus of elasticity (*Edyn*) was determined theoretically from the UPV values using the following equation:

$$Edyn = \frac{\rho\,(1+\mu)(1-2\mu)}{1-\mu}\,V^2 \qquad Eq.\ 3$$

where ρ is the density (kg/m^3), μ is the dynamic Poisson's ratio, and *V* is the pulse velocity (m/s) of concrete. The results of UPV and the calculated Edyn values are shown in Fig. 9. The SCC-R mixture had a velocity of 4460 m/s (44 GPa) at 3 days, which increased to 4900 m/s (52 GPa) at 91 days. The SCC-1 and SCC-2 mixtures showed nearly the same behavior: 4300 m/s (40 GPa) at 3 days followed by a low increase until the velocity reached that of the SCC-R mixture at 56 days. The stabilization after 56 days reflects the total CH consumed by the pozzolanic reaction. The evolution of velocity followed the ongoing hydration reactions of binder materials that formed a denser and interlocked microstructure. Overall, the UPV results indicated the good quality of concrete for the investigated SCC mixtures and agreed with the strength measurements.

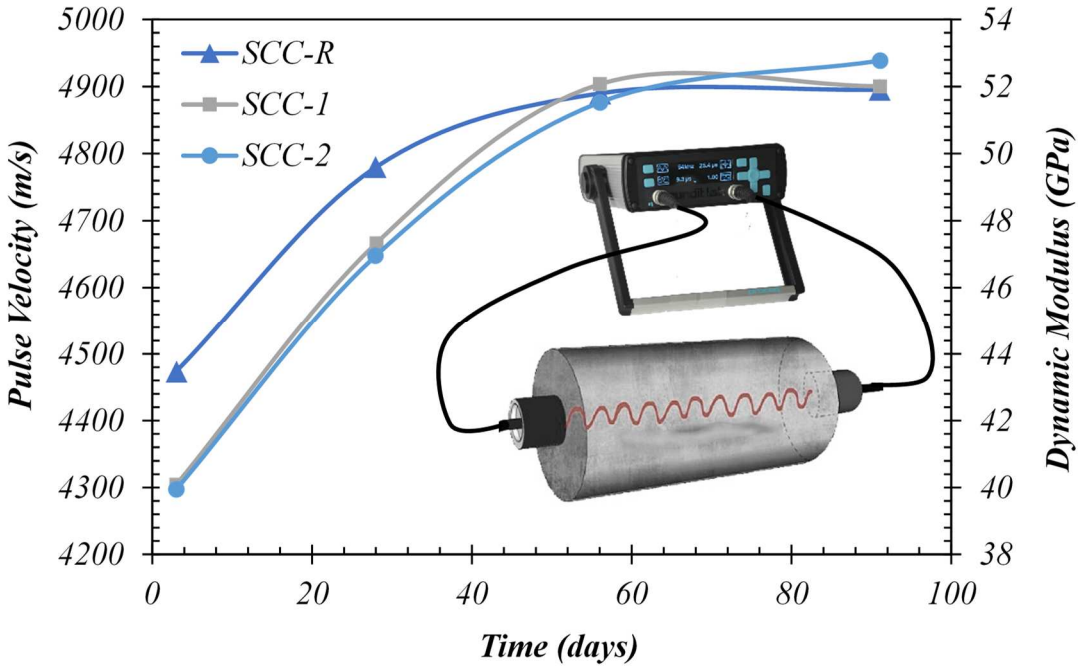

Fig. 9: UPV and E_{dyn} of the investigated SCC mixtures

302 ## 4.4. Microstructure characterization

303 ### 4.4.1. Mercury porosimetry

304 Microstructural and pore size distribution of the SCC mixtures were investigated. Fragments
305 taken from SCC mortar portions were dried at 105 °C for 24 h before mercury intrusion porosimetry
306 testing. The differential pore size distributions and the cumulative adsorption were calculated and
307 are illustrated in Fig. 10. The three SCC mixtures showed approximately the same pattern with
308 apparent diameters of most pores in the range of 5 to 50 nm. According to Cheng et al. (2018), the
309 pore structure can be divided into three major ranges: micro-pores (< 20 nm), meso-pores (20–200
310 nm), and macro-pores (> 200 nm), which is related to impermeability, less permeability, and high
311 permeability, respectively. Increasing the TMS content generated a shift in the differential curve
312 peak, which decreased the micro-pores from 32.3 nm to 21.1 and 26.3 nm for the SCC-1 and SCC-2
313 mixtures, respectively. This is shown clearly in the cumulative volume: the meso-pores increased,
314 which denotes that the pores became finer and denser.

315 According to Table 4, the SCC-1 mixture had the highest volume of micro-pores and the
316 lowest volume of meso-pores, followed by SCC-2 and SCC-R mixtures. A negligible volume of
317 macro-pores was observed in the three concrete samples, but it was mainly observed in the SCC-R
318 mixture. Although, the SCC-R mixture had the highest pore size, it exhibited a lower porosity
319 (8.74%) compared with the SCC-1 (9.08%) and SCC-2 samples (9.57%). Nevertheless, the small
320 particle size and high chemical activity of the TMS resulted in finer capillary porosity, which
321 increased the density, improved the structure, and reduced the volume of meso-pores and micro-
322 cracks. The porosity of the investigated mixtures indicates adequate durability because of the
323 optimization of the PD and the pozzolanic reaction of TMS which refined and increased the density
324 of ITZ.

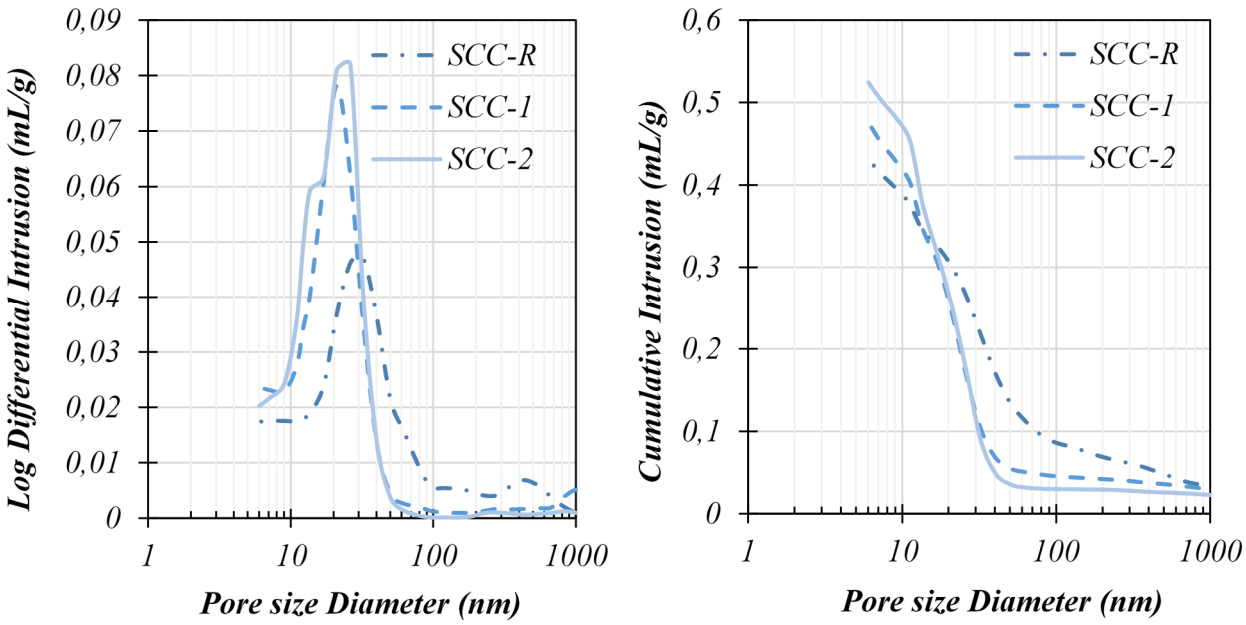

Fig. 10: Pore structure of SCC fragments at 91 days

Table 4: Pore size distribution of the investigated mixtures

Pore Ø (nm)		***Pore size distribution (%)***		
		SCC-R	***SCC-1***	***SCC-2***
Micro-pores	***< 20***	74.1	86.3	85.3
Meso-pores	***20 - 50***	22.7	13.2	14.5
	50 - 200	2.73	0.36	0.11
Macro-pores	***200 - 1000***	0.42	0.12	0.05
	> 1000	0.05	0.01	0.00

4.4.2. Interfacial transition zone

When the concrete is subjected to external forces, stresses are transferred to the ITZ. This factor is very important because the bonding between the cementitious paste and aggregates within the transition zone governs the concrete strength (Brandt, 1995). De Larrard and Belloc (1997) addressed a specific characteristic of the ITZ which is called the maximum paste thickness (MPT), which represents the mean distance between the contiguous CA as follows:

$$MPT = D_{max}\left(\sqrt[3]{\frac{g^*}{g}} - 1\right) \quad \text{where} \quad g^* = 1 - 0.45\left(\frac{d_{min}}{d_{max}}\right)^{0.19} \qquad Eq.\ 4$$

where D_{max} is the maximum size of aggregate (20 mm), g is the aggregate volume (0.266 m^3/m^3), g^* is equal to the PD of the aggregate, and d_{min} and d_{max} are the minimum and the maximum sizes of aggregate corresponding to 10 (0.18 mm) and 90% (8.86 mm) passing, respectively. MPT is considered a small-scale compressive strength test where the cementitious paste is the concrete specimen and the two juxtaposed CA are the test machine platens (T. de Grazia et al., 2019). A low MPT is associated with higher mechanical properties (Shadkam et al., 2017). The calculated MPT in this study was 8.70 mm, which is lower than those observed in previous studies (Shadkam et al., 2017; T. de Grazia et al., 2019).

To understand the formation of ITZ, the morphology characteristics of fragments of concrete were analyzed using a Hitachi S-4700 scanning electronic microscope (SEM). Fig. 11 represents the results of the coupled SEM-EDS analysis conducted on SCC-R and SCC-1 fragments. It was observed that the C-S-H mineral phases were well-formed, and large amounts of hydration products covered the particles forming a dense and homogeneous microstructure. However, for the SCC-2 mixture (Fig. 12) a disordered structure with a large amount of open pores was observed. In addition, numerous sulfate phases were detected in the SCC-2 mixture. This suggests that the ratio of calcium sulfate to tricalcium aluminate was high; otherwise, the ettringite tended to be replaced by calcium aluminate monosulfate phases. In addition, increasing the TMS content increased the calcium silicate content. Diverse CH crystallization was observed in the SCC-2, with thin hexagonal and globular shaped portlandite crystals (Alite and Belite) (Fig. 12-c) and a likewise rice particles of CH (Fig. 12-b). This fact confirms the low Ca/Si ratio at 20% of incorporation, which refers to the poor quality of the blended binder.

SEM and XRD analyses of the different SCCs demonstrated that increasing the TMS promoted the formation of ettringite, which may play an important role in the drying of the matrix and stabilization. The well formation of C-S-H improved the microstructure by improving the solid-

359 to-solid phase connectivity and reducing the pore-to-pore connectivity. Nevertheless, further
360 investigation of the thermodynamic modeling of blended cement-sediments is highly recommended.

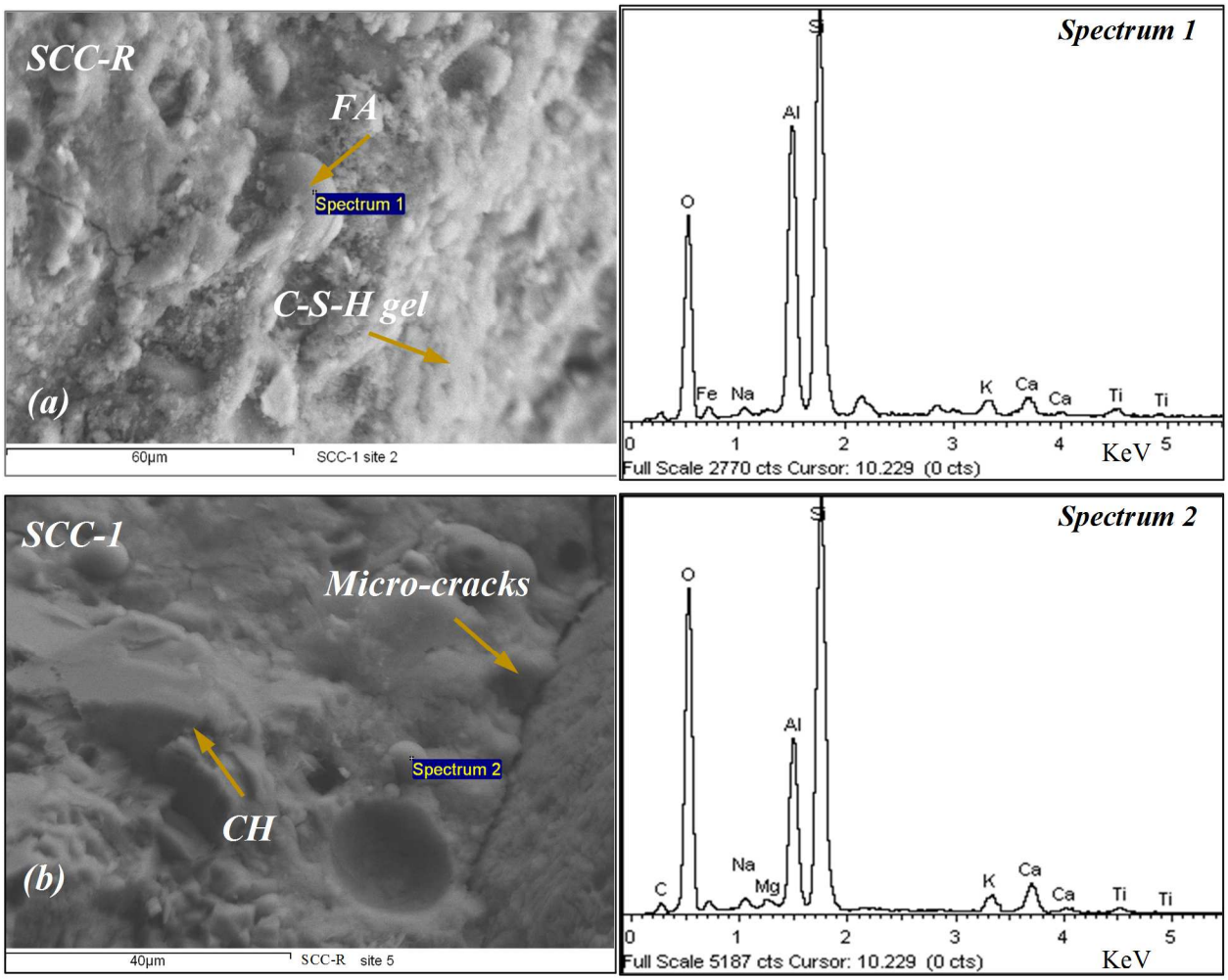

361

362 *Fig. 11: SEM-EDS with back-scattered electron analysis of SCC-R and SCC-1 at 91 days*

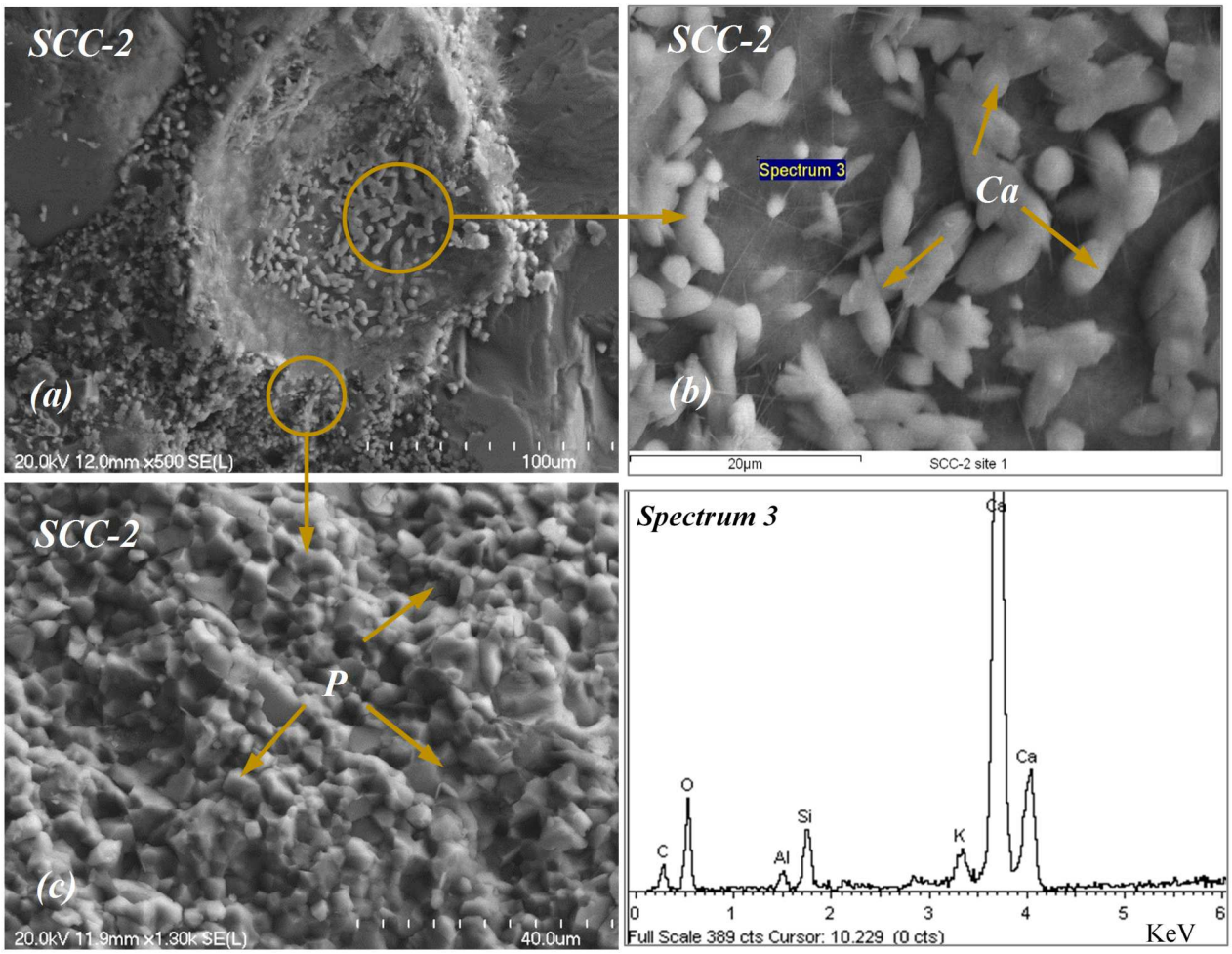

363

364 *Fig. 12: SEM-EDS with back-scattered electron analysis of SCC-2 at 91 days*

365 **4.5. Leaching test**

366 To analyze the mobility of trace elements (pollution indicators), a leaching test was
367 performed on ground fragments taken from the investigated SCC mixtures according to the NF EN
368 12457-2 (2002), using a liquid-to-solid ratio of 10:1 l/kg. The results are summarized in Table 5.
369 Increasing the TMS decreased the barium content in the matrix, which is a highly reactive and toxic
370 metal. A decrease in the concentrations of nickel, sulfates, and soluble fraction was noted as well. In
371 contrast, increasing the TMS content increased the concentration of chrome and chlorides.
372 Concentrations of As, Cd, Mo, Pb, Sb, Se, and Zn were below or close to the detection limits and
373 were in the same order of magnitude, which indicates that there was no significant change in the
374 chemistry and solubility. Overall, the concentration of trace elements in the ground powder of the

three SCCs was below the inert waste leaching limit according to the French Directive no. 0289 Published on December 14, 2014.

Table 5: Mobility of heavy metals (mg/kg) in the different SCCs

	SCC-R	***SCC-1***	***SCC-2***	***Limit***
As	< 0.08	< 0.08	< 0.08	0.50
Ba	9.33	2.99	2.78	20.0
Cd	< 0.01	< 0.01	< 0.01	0.04
Cr	0.01	0.19	0.22	0.50
Cu	0.03	0.06	0.05	2.00
Mo	< 0.06	0.08	0.08	0.50
Ni	0.14	< 0.06	< 0.06	0.40
Pb	< 0.03	< 0.03	< 0.03	0.50
Sb	< 0.06	< 0.06	< 0.06	0.06
Se	< 0.09	< 0.09	< 0.09	0.10
Zn	< 0.02	< 0.02	< 0.02	4.00
Fluorides	7.00	9.00	7.00	10.0
Chlorides	13.0	44.0	85.0	800
Sulfates	56.0	47.0	35.0	1000
Soluble Fraction	6057	5221	4835	4000

5. Conclusion

This study aimed to evaluate the influence of using treated marine sediments as SCM on the fresh, physical, hardened, microstructural, and environmental properties of SCC. Based on the experimental data, the following conclusions can be drawn:

1. The thermal treatment was efficient and led to an increase in the density and content of silicone dioxide (higher intensity of diffraction peaks of quartz) and a decrease in the content of sulfur trioxide.
2. The investigated SCC mixtures exhibited adequate self-consolidation characteristics with high filling ability, low T_{500}, high passing ability, and high stability for SCC production. The increase in TMS content did not significantly affect the workability.
3. TMS reduced the heat of binder hydration, which can be a positive effect in the case of mass concrete or a negative effect (early strength development) depending on the targeted application.
4. The investigated SCC mixtures showed similar strength development. The SCC-1 and SCC-2 mixtures exhibited a compressive strength of 66 ±1 MPa, which is similar to that of the reference mixture, at 91 days. Nevertheless, the SCC-2 mixture required a longer curing time to develop its mechanical properties. The results of the UPV agree with the strength findings and provided more insight into the development of internal microstructural micro-cracks in the investigated mixtures.
5. Microstructure development was improved by the incorporation of TMS. The SCC-1 mixture exhibited the highest volume of micro-pores, and the lowest volume of meso-pores, followed by the SCC-2 and SCC-R mixtures. The average total porosity of the three mixtures was approximately 9% with a standard deviation of 0.42%. This low porosity was mainly due to the pozzolanic reaction of the TMS which refined and increased the density of the ITZ.
6. The microscopic examinations indicated that an increase of TMS increased the content of calcium sulfate and calcium silicate. The SCC-1 and SCC-R mixtures showed similar well-formed ITZ. However, the microstructure of the SCC-2 mixture was disordered with a large amount of open pores. Increasing the content of TMS over 20% led to a negative microstructural effect.

7. The above findings, in addition to the leaching test result, should promote the valorization of dredged sediments in SCC as alternative SCM, thus contributing to the reduction of the carbon footprint of concrete production.

Acknowledgments

This research was carried out at the Department of civil and Building Engineering of the Université de Sherbrooke. It was funded by grants from Natural Sciences and Engineering Research Council of Canada (NSERC), and "Fonds de Recherche Nature et Technologies du Québec" (FRQNT), and The IMT Lille Douai. Authors would like to thank Sika Canada for providing the admixture, and Mr. Fantous Toufik for help in conducting the tests on SCC.

Declaration of Competing Interest

The authors declare that they have no known competing financial interests or personal relationships that could have appeared to influence the work reported in this paper.

CRediT authorship contribution statement

A. M. Safhi: Conceptualization, Data Curation, Formal analysis, Methodology, Validation, Visualization, Writing - Original Draft, Writing - Review & Editing. **P. Rivard**: Validation, Resources, Supervision, Project administration, Funding acquisition, Writing - Review & Editing. **A. Yahia**: Validation, Resources, Supervision, Writing - Review & Editing. **M. Benzerzour**: Resources, Project administration, Funding acquisition. **K. H. Khayat**: Validation, Writing - Review & Editing.

References

Abd Elrahman, M., Hillemeier, B., 2014. Combined effect of fine fly ash and packing density on the properties of high performance concrete: An experimental approach. Constr. Build. Mater. 58, 225–233. https://doi.org/10.1016/j.conbuildmat.2014.02.024

Aïssoun, B.M., Hwang, S.-D., Khayat, K.H., 2016. Influence of aggregate characteristics on workability of superworkable concrete. Mater. Struct. 49, 597–609. https://doi.org/10.1617/s11527-015-0522-9

Aouad, G., Laboudigue, A., Gineys, N., Abriak, N.E., 2012. Dredged sediments used as novel supply of raw material to produce Portland cement clinker. Cem. Concr. Compos. 34, 788–793. https://doi.org/10.1016/j.cemconcomp.2012.02.008

Ashrafian, A., Taheri Amiri, M.J., Rezaie-Balf, M., Ozbakkaloglu, T., Lotfi-Omran, O., 2018. Prediction of compressive strength and ultrasonic pulse velocity of fiber reinforced concrete incorporating nano silica using heuristic regression methods. Constr. Build. Mater. 190, 479–494. https://doi.org/10.1016/j.conbuildmat.2018.09.047

ASTM C29, 2017. Test Method for Bulk Density (Unit Weight) and Voids in Aggregate. ASTM International. https://doi.org/10.1520/C0029_C0029M-17A

ASTM C39, 2018. Test Method for Compressive Strength of Cylindrical Concrete Specimens. ASTM International. https://doi.org/10.1520/C0039_C0039M-18

ASTM C496, 2017. Test Method for Splitting Tensile Strength of Cylindrical Concrete Specimens. ASTM International. https://doi.org/10.1520/C0496_C0496M-17

ASTM C597, 2016. Test Method for Pulse Velocity Through Concrete. ASTM International. https://doi.org/10.1520/C0597-16

ASTM C1679, 2017. Practice for Measuring Hydration Kinetics of Hydraulic Cementitious Mixtures Using Isothermal Calorimetry. ASTM International. https://doi.org/10.1520/C1679-17

Benzerzour, M., Amar, M., Abriak, N.-E., 2017. New experimental approach of the reuse of dredged sediments in a cement matrix by physical and heat treatment. Constr. Build. Mater. 140, 432–444. https://doi.org/10.1016/j.conbuildmat.2017.02.142

Benzerzour, M., Maherzi, W., Amar, Mouhamadou.A.A., Abriak, N.-E., Damidot, D., 2018. Formulation of mortars based on thermally treated sediments. J. Mater. Cycles Waste Manag. 20, 592–603. https://doi.org/10.1007/s10163-017-0626-0

458 Bouhamou, N.-E., Mostefa, F., Mebrouki, A., Bendani, K., Belas, N., 2016. Influence of dredged
459 sediment on the shrinkage behavior of self-compacting concrete. Mater. Tehnol. 50, 127–
460 135. https://doi.org/10.17222/mit.2013.252
461 Brandt, A.M., 1995. Cement based composites: materials, mechanical properties and performance,
462 1. ed. ed. Spon, London.
463 Çakır, Ö., 2014. Experimental analysis of properties of recycled coarse aggregate (RCA) concrete
464 with mineral additives. Constr. Build. Mater. 68, 17–25.
465 https://doi.org/10.1016/j.conbuildmat.2014.06.032
466 Cheng, S., Shui, Z., Sun, T., Yu, R., Zhang, G., 2018. Durability and microstructure of coral sand
467 concrete incorporating supplementary cementitious materials. Constr. Build. Mater. 171,
468 44–53. https://doi.org/10.1016/j.conbuildmat.2018.03.082
469 Dang, T.A., Kamali-Bernard, S., Prince, W.A., 2013. Design of new blended cement based on
470 marine dredged sediment. Constr. Build. Mater. 41, 602–611.
471 https://doi.org/10.1016/j.conbuildmat.2012.11.088
472 De Larrard, F., Belloc, A., 1997. The influence of aggregate on the compressive strength of normal
473 and high-strength concrete. ACI Mater. J. 94, 417–426.
474 Ez-zaki, H., Diouri, A., 2019. Microstructural and physicomechanical properties of mortars-based
475 dredged sediment. Asian J. Civ. Eng. 20, 9–19. https://doi.org/10.1007/s42107-018-0084-6
476 Faure, A., Smith, A., Coudray, C., Anger, B., Colina, H., Moulin, I., Thery, F., 2017. Ability of
477 Two Dam Fine-Grained Sediments to be Used in Cement Industry as Raw Material for
478 Clinker Production and as Pozzolanic Additional Constituent of Portland-Composite
479 Cement. Waste Biomass Valorization 8, 2141–2163. https://doi.org/10.1007/s12649-017-
480 9870-8
481 Goltermann, P., Johansen, V., Palbøl, L., 1997. Packing of Aggregates: An Alternative Tool to
482 Determine the Optimal Aggregate Mix. Mater. J. 94, 435–443. https://doi.org/10.14359/328

Han, F., Liu, R., Wang, D., Yan, P., 2014. Characteristics of the hydration heat evolution of composite binder at different hydrating temperature. Thermochim. Acta 586, 52–57. https://doi.org/10.1016/j.tca.2014.04.010

Kasmi, A., Abriak, N.-E., Benzerzour, M., Azrar, H., 2017. Environmental impact and mechanical behavior study of experimental road made with river sediments: recycling of river sediments in road construction. J. Mater. Cycles Waste Manag. 19, 1405–1414. https://doi.org/10.1007/s10163-016-0529-5

Khayat, K.H., Assaad, J., Daczko, J., 2004. Comparison of Field-Oriented Test Methods to Assess Dynamic Stability of Self-Consolidating Concrete. ACI Mater. J. 101. https://doi.org/10.14359/13066

Khayat, K.H., Hu, C., Laye, J.-M., 2002. Importance of Aggregate Packing Density on Workability of Self-Consolidating Concrete, Proc., 1rst North American Conf. on the Design and Use of Self-Consolidating Concrete. Presented at the 1rst North American Conf. on the Design and Use of Self-Consolidating Concrete, Chicago, pp. 53–62.

Khayat, K.H., Hu, C., Monty, H., 1999. Stability of self compacting concrete, advantages, and potential applications, Proc., 1rst International RILEM Symposium on Self-Compacting Concrete. Presented at the 1rst International RILEM Symposium on Self-Compacting Concrete, RILEM Publications SARL, Stockholm, Sweden, pp. 143–152.

Laidani, Z.E.-A., Benabed, B., Abousnina, R., Gueddouda, M.K., Kadri, E.-H., 2020. Experimental investigation on effects of calcined bentonite on fresh, strength and durability properties of sustainable self-compacting concrete. Constr. Build. Mater. 230, 117062. https://doi.org/10.1016/j.conbuildmat.2019.117062

Lim, N.H.A.S., Mohammadhosseini, H., Tahir, M.Md., Samadi, M., Sam, A.R.M., 2018. Microstructure and Strength Properties of Mortar Containing Waste Ceramic Nanoparticles. Arab. J. Sci. Eng. 43, 5305–5313. https://doi.org/10.1007/s13369-018-3154-x

508 Liu, M., Wang, C., Bai, Y., Xu, G., 2018. Effects of sintering temperature on the characteristics of
509 lightweight aggregate made from sewage sludge and river sediment. J. Alloys Compd. 748,
510 522–527. https://doi.org/10.1016/j.jallcom.2018.03.216
511 Madrid, M., Orbe, A., Rojí, E., Cuadrado, J., 2017. The effects of by-products incorporated in low-
512 strength concrete for concrete masonry units. Constr. Build. Mater. 153, 117–128.
513 https://doi.org/10.1016/j.conbuildmat.2017.07.086
514 Mohammadhosseini, H., ABDUL AWAL, A.S.M., EHSAN, A.H., 2015. Influence of palm oil fuel
515 ash on fresh and mechanical properties of self-compacting concrete. Sadhana 40, 1989–
516 1999. https://doi.org/10.1007/s12046-015-0426-y
517 Mohammadhosseini, H., Tahir, M.Md., Mohd Sam, A.R., Abdul Shukor Lim, N.H., Samadi, M.,
518 2018. Enhanced performance for aggressive environments of green concrete composites
519 reinforced with waste carpet fibers and palm oil fuel ash. J. Clean. Prod. 185, 252–265.
520 https://doi.org/10.1016/j.jclepro.2018.03.051
521 Mohammadhosseini, H., Yatim, J.M., Sam, A.R.M., Awal, A.S.M.A., 2017. Durability performance
522 of green concrete composites containing waste carpet fibers and palm oil fuel ash. J. Clean.
523 Prod. 144, 448–458. https://doi.org/10.1016/j.jclepro.2016.12.151
524 Nanthagopalan, P., Santhanam, M., 2012. An empirical approach for the optimisation of aggregate
525 combinations for self-compacting concrete. Mater. Struct. 45, 1167–1179.
526 https://doi.org/10.1617/s11527-012-9824-3
527 NF EN 12457-2, 2002. Characterization of waste - Leaching - Compliance test for leaching of
528 granular waste materials and sludges - Part 2 : one stage batch test at a liquid to solid ratio of
529 10 l/kg for materials with particle size below 4 mm (without or with size reduction) -
530 Caractérisation des déchets. AFNOR.
531 Oey, T., Kumar, A., Bullard, J.W., Neithalath, N., Sant, G., 2013. The Filler Effect: The Influence
532 of Filler Content and Surface Area on Cementitious Reaction Rates. J. Am. Ceram. Soc. 96,
533 1978–1990. https://doi.org/10.1111/jace.12264

534 Rozas, F., Castillo, A., Martínez, I., Castellote, M., 2015. Guidelines for assessing the valorization
535 of a waste into cementitious material: dredged sediment for production of self compacting
536 concrete. Mater. Constr. 65, 057. https://doi.org/10.3989/mc.2015.10613
537 Rozière, E., Samara, M., Loukili, A., Damidot, D., 2015. Valorisation of sediments in self-
538 consolidating concrete: Mix-design and microstructure. Constr. Build. Mater. 81, 1–10.
539 https://doi.org/10.1016/j.conbuildmat.2015.01.080
540 Safhi, A. el M., Benzerzour, M., Rivard, P., Abriak, N.-E., 2018. Feasibility of using marine
541 sediments in SCC pastes as supplementary cementitious materials. Powder Technol.
542 https://doi.org/10.1016/j.powtec.2018.12.060
543 Safhi, A. el M., Benzerzour, M., Rivard, P., Abriak, N.-E., Ennahal, I., 2019. Development of self-
544 compacting mortars based on treated marine sediments. J. Build. Eng. 22, 252–261.
545 https://doi.org/10.1016/j.jobe.2018.12.024
546 Samara, M., Lafhaj, Z., Chapiseau, C., 2009. Valorization of stabilized river sediments in fired clay
547 bricks: Factory scale experiment. J. Hazard. Mater. 163, 701–710.
548 https://doi.org/10.1016/j.jhazmat.2008.07.153
549 Sedran, T., Larrard, F.D., Guen, L.L., 2007. Détermination de la compacité des ciments et additions
550 minérales à la sonde de Vicat. Bull. Lab. Ponts Chaussées 155–163.
551 Self-Compacting Concrete European Project Group, 2005. The European Guidelines for Self-
552 compacting Concrete: Specification, Production and Use. International Bureau for Precast
553 Concrete (BIBM).
554 Shadkam, H.R., Dadsetan, S., Tadayon, M., Sanchez, L.F.M., Zakeri, J.A., 2017. An investigation
555 of the effects of limestone powder and Viscosity Modifying Agent in durability related
556 parameters of self-consolidating concrete (SCC). Constr. Build. Mater. 156, 152–160.
557 https://doi.org/10.1016/j.conbuildmat.2017.08.165
558 Siavalas, G., Werner, D., Karapanagioti, H.K., Bowler, B.F.J., Manning, D.A.C., Christanis, K.,
559 2013. Comparison of methods for the characterization and quantification of carbon forms in

estuarine and marine sediments from coal mining regions. Org. Geochem. 59, 61–74. https://doi.org/10.1016/j.orggeochem.2013.03.007

Skaropoulou, A., Sotiriadis, K., Kakali, G., Tsivilis, S., 2013. Use of mineral admixtures to improve the resistance of limestone cement concrete against thaumasite form of sulfate attack. Cem. Concr. Compos. 37, 267–275. https://doi.org/10.1016/j.cemconcomp.2013.01.007

Snellings, R., Cizer, Ö., Horckmans, L., Durdziński, P.T., Dierckx, P., Nielsen, P., Van Balen, K., Vandewalle, L., 2016. Properties and pozzolanic reactivity of flash calcined dredging sediments. Appl. Clay Sci. 129, 35–39. https://doi.org/10.1016/j.clay.2016.04.019

Snellings, R., Horckmans, L., Van Bunderen, C., Vandewalle, L., Cizer, Ö., 2017. Flash-calcined dredging sediment blended cements: effect on cement hydration and properties. Mater. Struct. 50, 241. https://doi.org/10.1617/s11527-017-1108-5

T. de Grazia, M., F. M. Sanchez, L., C. O. Romano, R., G. Pileggi, R., 2019. Investigation of the use of continuous particle packing models (PPMs) on the fresh and hardened properties of low-cement concrete (LCC) systems. Constr. Build. Mater. 195, 524–536. https://doi.org/10.1016/j.conbuildmat.2018.11.051

Van Bunderen, C., Snellings, R., Horckmans, L., Vandewalle, L., Cizer, Ö., 2017. Mixture Proportions of Concrete with Dredging Sediments as Novel SCM. Spec. Publ. 320, 27.1-27.10.

Van Bunderen, C., Snellings, R., Vandewalle, L., Cizer, Ö., 2019. Early-age hydration and autogenous deformation of cement paste containing flash calcined dredging sediments. Constr. Build. Mater. 200, 104–115. https://doi.org/10.1016/j.conbuildmat.2018.12.090

Wong, H. s., Zobel, M., Buenfeld, N. r., Zimmerman, R. w., 2009. Influence of the interfacial transition zone and microcracking on the diffusivity, permeability and sorptivity of cement-based materials after drying. Mag. Concr. Res. 61, 571–589. https://doi.org/10.1680/macr.2008.61.8.571

585 Xu, Y., Yan, C., Xu, B., Ruan, X., Wei, Z., 2014. The use of urban river sediments as a primary raw
586 material in the production of highly insulating brick. Ceram. Int. 40, 8833–8840.
587 https://doi.org/10.1016/j.ceramint.2014.01.105
588 Zhao, Z., Benzerzour, M., Abriak, N.-E., Damidot, D., Courard, L., Wang, D., 2018. Use of
589 uncontaminated marine sediments in mortar and concrete by partial substitution of cement.
590 Cem. Concr. Compos. 93, 155–162. https://doi.org/10.1016/j.cemconcomp.2018.07.010
591